Magnetoconductance of rectangular arrays of quantum rings

Orsolya Kálmán,[1,2] Péter Földi,[2] Mihály G. Benedict,[2,*] and F. M. Peeters[3]
[1]*Department of Quantum Optics and Quantum Information, Research Institute for Solid State Physics and Optics, Hungarian Academy of Sciences, Konkoly-Thege Miklós út 29-33, H-1121 Budapest, Hungary*
[2]*Department of Theoretical Physics, University of Szeged, Tisza Lajos körút 84, H-6720 Szeged, Hungary*
[3]*Departement Fysica, Universiteit Antwerpen, Groenenborgerlaan 171, B-2020 Antwerpen, Belgium*
(Received 22 April 2008; revised manuscript received 30 June 2008; published 4 September 2008)

Electron transport through multiterminal rectangular arrays of quantum rings is studied in the presence of Rashba-type spin-orbit interaction (SOI) and of a perpendicular magnetic field. Using the analytic expressions for the transmission and reflection coefficients for single rings we obtain the conductance through such arrays as a function of the SOI strength, of the magnetic flux, and of the wave vector k of the incident electron. Due to destructive or constructive spin interferences caused by the SOI, the array can be totally opaque for certain ranges of k, while there are parameter values where it is completely transparent. Spin resolved transmission probabilities show nontrivial spin transformations at the outputs of the arrays. When pointlike random scattering centers are placed between the rings, the Aharonov-Bohm peaks split, and an oscillatory behavior of the conductance emerges as a function of the SOI strength.

DOI: 10.1103/PhysRevB.78.125306 PACS number(s): 73.23.Ad, 03.65.−w, 85.35.Ds, 71.70.Ej

I. INTRODUCTION

Magnetoconductance oscillations of quantum rings made of semiconducting materials[1] exhibiting Rashba-type spin-orbit interaction[2–4] (SOI) have been intensely studied in the past few years. These effects are manifestations of flux- and spin-dependent quantum interference phenomena. In view of the possible spintronic applications and the conceptual importance of these interference effects in multiply-connected domains, closed single-quantum rings (without attached leads)[5–8] as well as two- or three-terminal ones were investigated[9–22] extensively. Additionally, the conductance properties of a linear chain of rings have also been determined.[23]

In this paper we present a method that enables one to calculate the conductance and the spin transport properties of two-dimensional rectangular arrays consisting of quantum rings with Rashba-type SOI (Ref. 24) and with a perpendicular magnetic field. Such arrays, fabricated from, e.g., an InAlAs/InGaAs based two-dimensional electron gas (2DEG),[25] have been studied in a recent experiment[26] and in a subsequent theoretical work[27] to demonstrate the time-reversal Aharonov-Casher effect.[28] Here we present a more general survey of the magnetoconductance properties of such devices, including the perturbative treatment of the magnetic field which still allows us to analytically solve the scattering problem in case of two-, three-, and four-terminal rings, which are then used as building blocks of larger arrays. We also present results related to the spin-resolved transmission properties of the network, which is an issue that has not been addressed so far. Our method is based on analytic results and can be used for an arbitrary configuration. For the sake of definiteness, we consider 3×3, 4×4, and 5×5 rectangular arrays,[26,27] which are closed in the vertical and open in the horizontal direction. Additionally, we study the magnetoconductance properties and spin-resolved transmission probabilities of the same array geometry with only one input channel. We also investigate to what extent the conductance properties are modified by the presence of pointlike random scattering centers between the rings. In our calculations we assume that the rings are narrow enough to be considered one dimensional and the transport of the electrons through the arrays is ballistic. We determine the magnetoconductance in the framework of the Landauer-Büttiker formalism.[29]

Rectangular arrays[26,27]—depending on the number of input leads—consist of two-, three-, and four-terminal rings (see Fig. 1), where the two- and three-terminal ones are situated on the boundary of the arrays as shown in Fig. 2 with or without the input leads displayed by dashed lines. The transmission and reflection properties of two- and three-terminal rings have been determined in previous works[10–12,14,30–35] but the effect of the magnetic field on the spin degree of freedom has not been taken into account for an arbitrary geometry. Additionally, the most general boundary condition that is required by this two-dimensional problem has not been investigated so far. Therefore in Sec. II we first consider a perpendicular magnetic field as a weak perturbation, then, in order to account for all possible reflections and transmissions when building up the array from single rings, we generalize our previous results to the case when electrons can enter/exit on any of the terminals of a three-terminal ring (results for two- and four-terminal rings are presented in Appendix). Next, in Sec. III A the individual rings are used as building blocks of the arrays by fitting the wave functions and their derivatives in the points where neighboring rings touch each other. Magnetoconductance properties are presented here as a function of the wave number k of the incoming electron, the magnetic flux, and the SOI strength. Spin resolved transmission probabilities on the output side of the arrays are also derived. In Sec. III B we investigate the effect of random Dirac-delta scattering potentials in between the rings.

II. BUILDING BLOCKS OF TWO-DIMENSIONAL ARRAYS: SINGLE QUANTUM RINGS

In this section we consider a single narrow quantum ring[31] of radius a located in the xy plane in the presence of Rashba

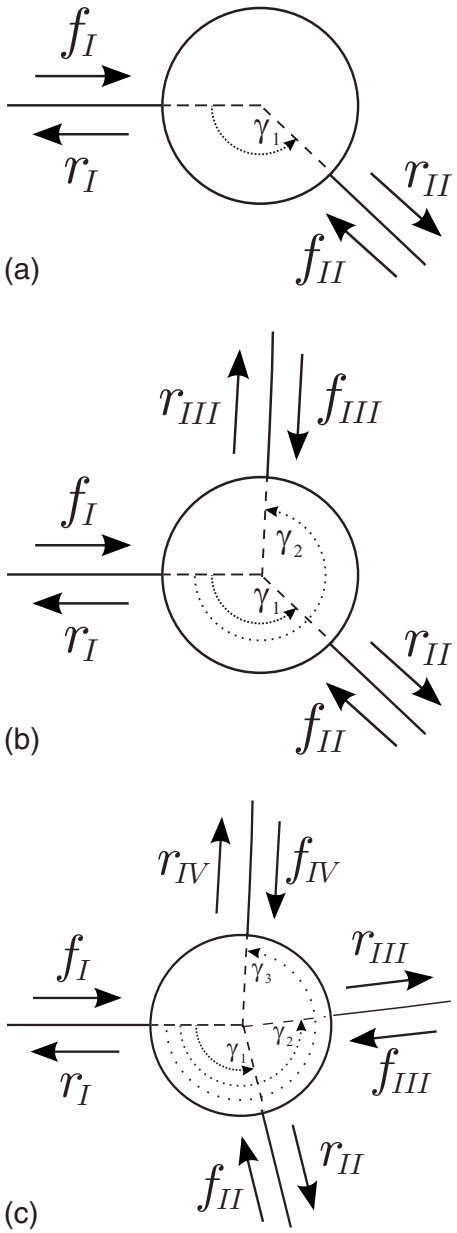

FIG. 1. The notations used for the spinor part of the wave functions in the case of (a) two-, (b) three-, and (c) four-terminal rings.

SOI (Ref. 24) and a perpendicular magnetic field B. If B is relatively weak, then the interaction between the electron spin and the field, i.e., the Zeeman term, can be treated as a perturbation and the relevant dimensionless Hamiltonian reads[11,36]

$$H = \left[\left(-i\frac{\partial}{\partial\varphi} - \frac{\Phi}{\Phi_0} + \frac{\omega_{\mathrm{SO}}}{2\Omega}\sigma_r\right)^2 - \frac{\omega_{\mathrm{SO}}^2}{4\Omega^2}\right] + H_p, \qquad (1)$$

where φ is the azimuthal angle of a point on the ring, Φ denotes the magnetic flux encircled by the ring, $\Phi_0 = h/e$ is the unit flux, and $\omega_{\mathrm{SO}} = \alpha/\hbar a$ is the frequency associated with the spin-orbit interaction. $\hbar\Omega = \hbar^2/2m^*a^2$ characterizes the kinetic energy with m^* being the effective mass of the electron, and the radial spin operator is given by $\sigma_r = \sigma_x \cos\varphi + \sigma_y \sin\varphi$. The perturbative term H_p is given by[11]

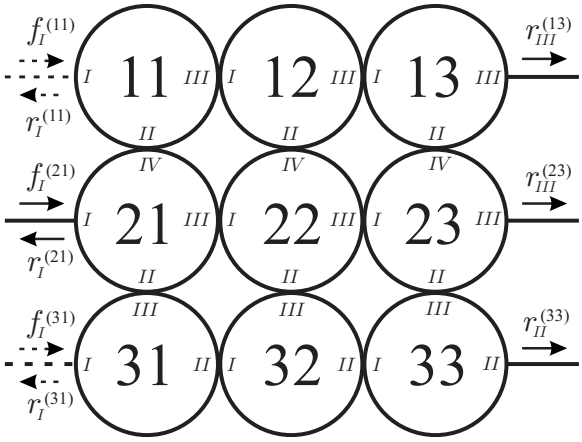

FIG. 2. The geometry of the device in the simplest case of a 3 $\times$3 array with three or one (without leads displayed with dashed lines) input terminals. The notations can easily be generalized to larger arrays.

$$H_p = \frac{\omega_L}{\Omega}\sigma_z,$$

where $\omega_L = g^* eB/4m$, with g^* and m being the effective gyromagnetic ratio and the free-electron mass, respectively.

The energy eigenvalues of the unperturbed Hamiltonian are

$$E_0^{(\mu)}(\kappa) = \left(\kappa - \frac{\Phi}{\Phi_0}\right)^2 + (-1)^\mu\left(\kappa - \frac{\Phi}{\Phi_0}\right)w + \frac{1}{4} \quad (\mu = 1,2), \qquad (2a)$$

and the corresponding eigenvectors in the $|\uparrow_z\rangle, |\downarrow_z\rangle$ eigenbasis of σ_z read

$$\psi^{(\mu)}(\kappa,\varphi) = e^{i\kappa\varphi}\begin{pmatrix} e^{-i\varphi/2}u^{(\mu)} \\ e^{i\varphi/2}v^{(\mu)} \end{pmatrix}, \qquad (2b)$$

where $u^{(1)} = -v^{(2)} = \cos(\theta/2)$, $u^{(2)} = v^{(1)} = \sin(\theta/2)$, and

$$\tan(\theta/2) = \frac{\Omega}{\omega_{\mathrm{SO}}}(1-w), \qquad (3)$$

with $w = \sqrt{1+\omega_{\mathrm{SO}}^2/\Omega^2}$. The matrix elements of H_p in the basis of these eigenstates are obtained as

$$\langle\psi^{(\mu)}|H_p|\psi^{(\mu)}\rangle = (-1)^{\mu+1}\frac{\omega_L}{\Omega}\cos\theta = (-1)^{\mu+1}\frac{\omega_L}{\Omega}\frac{1}{w},$$

$$\langle\psi^{(1)}|H_p|\psi^{(2)}\rangle = \frac{\omega_L}{\Omega}\sin\theta.$$

In the first-order approximation one neglects the off-diagonal elements; this is reasonable if they are small, i.e., if $\omega_L/\Omega \ll k^2a^2$, where k denotes the wave number of the incident electron, which is described as a plane wave. Within this approximation, the eigenspinors are not perturbed and their direction is still specified by the angle θ given by Eq. (3).

The energy eigenvalues including the first-order corrections are given by

$$E^{(\mu)}(\kappa) = E_0^{(\mu)}(\kappa) + (-1)^{\mu+1}\frac{\omega_L}{\Omega}\frac{1}{w}.$$

Imposing the condition of energy conservation $k^2a^2 = E^{(\mu)}(\kappa)$ determines the possible values of κ,

$$\kappa_j^{(\mu)} = (-1)^{\mu+1}\left[\frac{w}{2} + (-1)^j q^{(\mu)}\right] + \frac{\Phi}{\Phi_0},$$

where $\mu, j = 1, 2$ and

$$q^{(\mu)} = \sqrt{q^2 + (-1)^{\mu}\frac{\omega_L}{\Omega}\frac{1}{w}}, \tag{4}$$

with $q = \sqrt{(\omega_{SO}/2\Omega)^2 + E/\hbar\Omega}$, where $E = \hbar^2k^2/2m^*$ denotes the energy of the incoming electron. The corresponding four eigenspinors read

$$\psi_j^{(1)}(\kappa_j^{(1)}, \varphi) = e^{i\kappa_j^{(1)}\varphi}\begin{pmatrix} e^{-i\varphi/2}\cos(\theta/2) \\ e^{i\varphi/2}\sin(\theta/2) \end{pmatrix}, \tag{5}$$

$$\psi_j^{(2)}(\kappa_j^{(2)}, \varphi) = e^{i\kappa_j^{(2)}\varphi}\begin{pmatrix} e^{-i\varphi/2}\sin(\theta/2) \\ -e^{i\varphi/2}\cos(\theta/2) \end{pmatrix}. \tag{6}$$

The wave functions belonging to the same energy in the different sections of the ring are linear combinations of these eigenspinors.

The building blocks of the rectangular arrays we investigate are two-, three-, and four-terminal quantum rings (see Fig. 1), where, in general, the boundary conditions allow both incoming and outgoing spinor valued wave functions at each terminal: $\Psi_i = f_i e^{ikx_i} + r_i e^{-ikx_i}$ $(i = \mathrm{I}, \mathrm{II}, \mathrm{III}, \mathrm{IV})$, where x_i denotes the local coordinate in terminal i. Note that the amplitudes $f_\mathrm{I}, r_\mathrm{I}, f_\mathrm{II}, \cdots$ refer to two-component spinors, e.g.,

$$f_\mathrm{I} = \begin{pmatrix} (f_\mathrm{I})_\uparrow \\ (f_\mathrm{I})_\downarrow \end{pmatrix}.$$

For the sake of definiteness, we focus on a general three-terminal ring, shown in Fig. 1(b). The scattering problem in the case of a ring with four terminals [Fig. 1(c)] can also be solved analytically, as presented in Appendix, where we also give the results for a general two-terminal ring [Fig. 1(a)]. The outgoing spinors $(r_i, i = \mathrm{I}, \mathrm{II}, \mathrm{II})$ are connected to the incoming ones (f_i) by 2×2 matrices, which can be determined by requiring the continuity of the wave functions and vanishing net spin current densities (Griffith conditions)[11,13,32,37] at the junctions. For the same boundary conditions as in Ref. 35, i.e., for $f_\mathrm{II}, f_\mathrm{III} = 0$ in Fig. 1(b), the reflection matrix which connects r_I to the incoming spinor f_I is given by

$$R_{\uparrow\uparrow}^{f_\mathrm{I}} = \varrho^{(1)}\cos^2(\theta/2) + \varrho^{(2)}\sin^2(\theta/2) - 1,$$

$$R_{\uparrow\downarrow}^{f_\mathrm{I}} = (\varrho^{(1)} - \varrho^{(2)})\sin(\theta/2)\cos(\theta/2),$$

$$R_{\downarrow\uparrow}^{f_\mathrm{I}} = R_{\uparrow\downarrow}^{f_\mathrm{I}},$$

$$R_{\downarrow\downarrow}^{f_\mathrm{I}} = \varrho^{(1)}\sin^2(\theta/2) + \varrho^{(2)}\cos^2(\theta/2) - 1, \tag{7}$$

where

$$\begin{aligned}\varrho^{(\mu)} = 8ka/y^{(\mu)}\{&-i(q^{(\mu)})^2\sin(2q^{(\mu)}\pi) \\ &- kaq^{(\mu)}[\sin(q^{(\mu)}\gamma_1)\sin(q^{(\mu)}(2\pi - \gamma_1)) \\ &+ \sin(q^{(\mu)}\gamma_2)\sin(q^{(\mu)}(2\pi - \gamma_2))] \\ &+ ik^2a^2\sin(q^{(\mu)}\gamma_1)\sin(q^{(\mu)}(\gamma_2 - \gamma_1)) \\ &\times\sin(q^{(\mu)}(2\pi - \gamma_2))\},\end{aligned}$$

and

$$\begin{aligned}y^{(\mu)} = {}& 8(q^{(\mu)})^3\{\cos[[(-1)^{\mu+1}w + 2\phi]\pi] + \cos(2q^{(\mu)}\pi)\} \\ &- 12ika(q^{(\mu)})^2\sin(2q^{(\mu)}\pi) + 4k^2a^2q^{(\mu)}\cos[2q^{(\mu)}\pi] \\ &- 2k^2a^2q^{(\mu)}\{\cos[2q^{(\mu)}(\pi - \gamma_2 + \gamma_1)] - \cos(2q^{(\mu)}\pi) \\ &+ \cos[2q^{(\mu)}(\pi - \gamma_2)] + \cos[2q^{(\mu)}(\pi - \gamma_1)]\} \\ &+ ik^3a^3\{\sin[2q^{(\mu)}(\pi - \gamma_2 + \gamma_1)] - \sin[2q^{(\mu)}\pi] \\ &+ \sin[2q^{(\mu)}(\pi - \gamma_1)] - \sin[2q^{(\mu)}(\pi - \gamma_2)]\},\end{aligned}$$

with $\phi = \Phi/\Phi_0$. The matrices describing the connection between the outgoing spinors r_II, r_III and the input f_I—the so-called transmission matrices—are given by

$$(T_n^{f_\mathrm{I}})_{\uparrow\uparrow} = e^{-i\gamma_n/2}(\tau_n^{(1)}\cos^2(\theta/2) + \tau_n^{(2)}\sin^2(\theta/2)),$$

$$(T_n^{f_\mathrm{I}})_{\uparrow\downarrow} = e^{-i\gamma_n/2}(\tau_n^{(1)} - \tau_n^{(2)})\sin(\theta/2)\cos(\theta/2),$$

$$(T_n^{f_\mathrm{I}})_{\downarrow\uparrow} = e^{i\gamma_n/2}(\tau_n^{(1)} - \tau_n^{(2)})\sin(\theta/2)\cos(\theta/2),$$

$$(T_n^{f_\mathrm{I}})_{\downarrow\downarrow} = e^{i\gamma_n/2}(\tau_n^{(1)}\sin^2(\theta/2) + \tau_n^{(2)}\cos^2(\theta/2)), \tag{8}$$

where $n = 1, 2$, indicating the two possible output channels, and

$$\begin{aligned}\tau_1^{(\mu)} = {}& \frac{8kaq^{(\mu)}}{y^{(\mu)}}e^{i\gamma_1/2((-1)^{\mu+1}w + 2\phi)} \\ &\times\{-ka\sin(q^{(\mu)}(\gamma_2 - \gamma_1))\sin(q^{(\mu)}(2\pi - \gamma_2)) \\ &+ iq^{(\mu)}[e^{-i\pi((-1)^{\mu+1}w + 2\phi)}\sin(q^{(\mu)}\gamma_1) \\ &- \sin(q^{(\mu)}(2\pi - \gamma_1))]\},\end{aligned}$$

$$\begin{aligned}\tau_2^{(\mu)} = {}& \frac{8kaq^{(\mu)}}{y^{(\mu)}}e^{i\gamma_2/2((-1)^{\mu+1}w + 2\phi)} \\ &\times\{kae^{-i\pi((-1)^{\mu+1}w + 2\phi)}\sin(q^{(\mu)}\gamma_1)\sin(q^{(\mu)}(\gamma_2 - \gamma_1)) \\ &+ iq^{(\mu)}[e^{-i\pi((-1)^{\mu+1}w + 2\phi)}\sin(q^{(\mu)}\gamma_2) \\ &- \sin(q^{(\mu)}(2\pi - \gamma_2))]\}.\end{aligned}$$

Note that the boundary conditions applied to obtain the R^{f_I} and $T_n^{f_\mathrm{I}}$ matrices above are similar to that of Ref. 35. However the magnetic field induced shift of the spin Zeeman levels leads to a doubling of the parameters according to Eq. (4). This modifies significantly the physical transport properties of the device.

Let us point out that having obtained the matrix elements above is enough to handle the problem with both incoming

and outgoing waves on all terminals of the ring as shown in Fig. 1(b). Namely, we can consider the three inputs f_i ($i=\mathrm{I},\mathrm{II},\mathrm{III}$) separately and determine the corresponding reflection and transmission matrices. The outputs in the superposed problem will consist of contributions from all inputs: the reflected part of the spinor which enters on the same lead and the transmitted parts of the other two inputs into the respective lead,

$$r_{\mathrm{I}} = R^{f_{\mathrm{I}}} f_{\mathrm{I}} + T_2^{f_{\mathrm{II}}} f_{\mathrm{II}} + T_1^{f_{\mathrm{III}}} f_{\mathrm{III}},$$

$$r_{\mathrm{II}} = T_1^{f_{\mathrm{I}}} f_{\mathrm{I}} + R^{f_{\mathrm{II}}} f_{\mathrm{II}} + T_2^{f_{\mathrm{III}}} f_{\mathrm{III}},$$

$$r_{\mathrm{III}} = T_2^{f_{\mathrm{I}}} f_{\mathrm{I}} + T_1^{f_{\mathrm{II}}} f_{\mathrm{II}} + R^{f_{\mathrm{III}}} f_{\mathrm{III}}. \tag{9}$$

Considering f_{II} (f_{III}) as the only input, the reflection and transmission matrices are the same as those for the input f_{I}, except for the appropriate changes in the angles, since in the reference frame of f_{II} (f_{III}), the angles of the output leads are measured from the lead through which f_{II} (f_{III}) enters the ring. In order to get the contributions to the output spinors for the input f_{II} (f_{III}) in the reference frame of f_{I}, the matrices need to be rotated [see Fig. 1(b)] by the angle of $\gamma_1(\gamma_2)$,

$$M^{f_{\mathrm{II}}} = U_{\gamma_1} M^{f_{\mathrm{I}}}_{\gamma_1 \leftrightarrow \gamma_2 - \gamma_1,\ \gamma_2 \leftrightarrow 2\pi - \gamma_1} U^{-1}_{\gamma_1}, \tag{10}$$

$$M^{f_{\mathrm{III}}} = U_{\gamma_2} M^{f_I}_{\gamma_1 \leftrightarrow 2\pi - \gamma_2,\ \gamma_2 \leftrightarrow 2\pi - \gamma_2 + \gamma_1} U^{-1}_{\gamma_2}, \tag{11}$$

where $M = R, T_1, T_2$ and

$$U_{\gamma_n} = \begin{pmatrix} e^{-i\gamma_n/2} & 0 \\ 0 & e^{i\gamma_n/2} \end{pmatrix}, \quad n = 1,2.$$

The above approach is also valid in the case of the two- and four-terminal rings. Using the reflection and transmission matrices as presented in Appendix, the more general problem of having both incoming and outgoing waves on all terminals can easily be treated. All possible reflections and transmissions can thus be taken into account when forming two-dimensional arrays of such rings.

III. RECTANGULAR ARRAYS OF QUANTUM RINGS

A. Magnetoconductance properties

Based on the analytic results presented in Sec. II and in Appendix we may build $\mathrm{M}\times\mathrm{M}$ two-dimensional rectangular arrays of quantum rings, where both perpendicular electric and magnetic fields are present, so that the former one can be used to change the strength of the SOI.[3] Here we focus on of 3×3, 4×4, and 5×5 arrays and assume that neighboring rings touch each other. In addition, we limit ourselves to arrays that are closed in the vertical and open in the horizontal direction, as shown in Fig. 2. Two types of such arrays will be investigated: (i) the electron can enter/exit the array through any of the rings in the horizontal direction and (ii) the electron can enter the array through one ring only (no leads are attached to the other rings on the entrance side) but can exit through any of the rings on the opposite side (Fig. 2 without the dashed curves). In both cases the conductance is derived from the linear set of equations resulting from the fit of the wave functions $\Psi_i^{(kl)}$ ($i=\mathrm{I},\mathrm{II},\mathrm{III},\mathrm{IV}$ and $k,l=1,\ldots,N$, where N is the number of rings along one direction in the array) and their derivatives $\partial_{x_i^{(kl)}}\Psi_i^{(kl)}$ in the points, where the rings touch each other, for example,

$$\Psi_{\mathrm{III}}^{(11)}\big|_{x_{\mathrm{III}}^{(11)}=0} = \Psi_{\mathrm{I}}^{(12)}\big|_{x_I^{(12)}=0},$$

$$\partial_{x_{\mathrm{III}}^{(11)}}\Psi_{\mathrm{III}}^{(11)}\big|_{x_{\mathrm{III}}^{(11)}=0} = -\partial_{x_{\mathrm{I}}^{(12)}}\Psi_{\mathrm{I}}^{(12)}\big|_{x_{\mathrm{I}}^{(12)}=0}. \tag{12}$$

Here we used the notations of Fig. 2. (Note that the negative sign in Eq. (12) is a consequence of the opposite direction of the local coordinates in leads III of ring {11} and I of ring {12}.) Equation (12) leads to

$$f_{\mathrm{III}}^{(11)} + r_{\mathrm{III}}^{(11)} = f_{\mathrm{I}}^{(12)} + r_{\mathrm{I}}^{(12)},$$

$$f_{\mathrm{III}}^{(11)} - r_{\mathrm{III}}^{(11)} = -f_{\mathrm{I}}^{(12)} + r_{\mathrm{I}}^{(12)},$$

from which follows that

$$f_{\mathrm{III}}^{(11)} = r_{\mathrm{I}}^{(12)},$$

$$r_{\mathrm{III}}^{(11)} = f_I^{(12)},$$

i.e., the spinor entering (exiting) ring {11} on terminal III is equal to the spinor exiting (entering) ring {12} on terminal I. The spinors $r_{\mathrm{III}}^{(11)}$ and $r_{\mathrm{I}}^{(12)}$ can be given with the help of the reflection and transmission matrices of a three-terminal ring according to Eq. (9).

For a small number of rings the resulting set of equations can be solved analytically; however already for an array of 3×3 rings shown in Fig. 2, it consists of 60 equations, which is preferably solved by numerical means, although analytic solutions exist in principle. (For larger arrays the number of equations scales practically with the number of rings.) After having determined the output spinor valued wave functions $r_{\mathrm{III}}^{(1N)}, r_{\mathrm{III}}^{(2N)}, \ldots, r_{\mathrm{II}}^{(NN)}$, where N is the number of rings in the horizontal direction, the Landauer-Büttiker[29] formula

$$G = G_\uparrow + G_\downarrow,$$

where

$$G_\uparrow = \frac{e^2}{h}\left(\left|\left(r_{\mathrm{III}}^{(1N)}\right)_\uparrow\right|^2 + \left|\left(r_{\mathrm{III}}^{(2N)}\right)_\uparrow\right|^2 + \cdots + \left|\left(r_{\mathrm{II}}^{(NN)}\right)_\uparrow\right|^2\right),$$

$$G_\downarrow = \frac{e^2}{h}\left(\left|\left(r_{\mathrm{III}}^{(1N)}\right)_\downarrow\right|^2 + \left|\left(r_{\mathrm{III}}^{(2N)}\right)_\downarrow\right|^2 + \cdots + \left|\left(r_{\mathrm{II}}^{(NN)}\right)_\downarrow\right|^2\right)$$

are used to calculate the conductance of the arrays, averaged over the two σ_z eigenspinor inputs. We note that our method of using single rings as building blocks can easily be used to determine the conductance of arrays of arbitrary—not necessarily rectangular—configuration as well.

Figure 3 shows a contour plot of the conductance (in e^2/h units) of rectangular arrays of 3×3, 4×4, and 5×5 quantum rings for zero magnetic flux as a function of the SOI

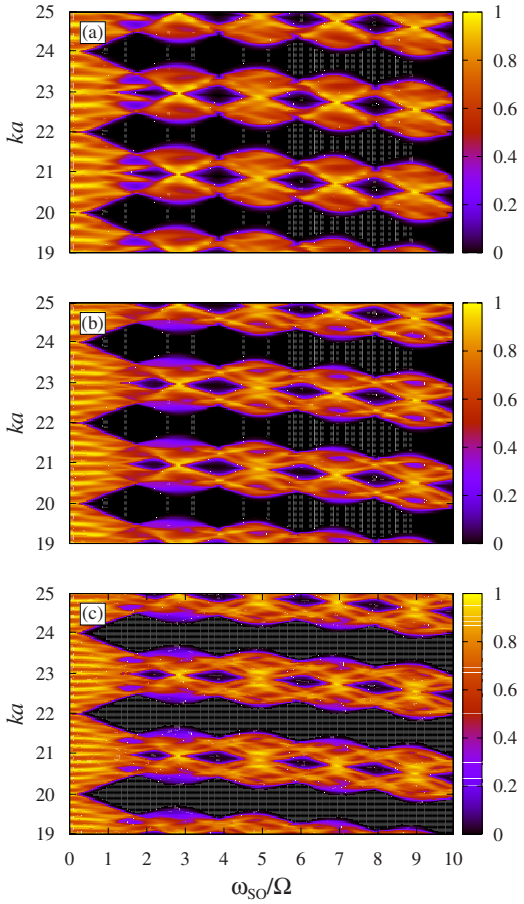

FIG. 3. (Color online) The conductance G/G_0 ($G_0=e^2/h$) of (a) 3×3, (b) 4×4, and (c) 5×5 rectangular arrays with 3, 4, and 5 input terminals, respectively, for zero magnetic flux as a function of the SOI strength and ka.

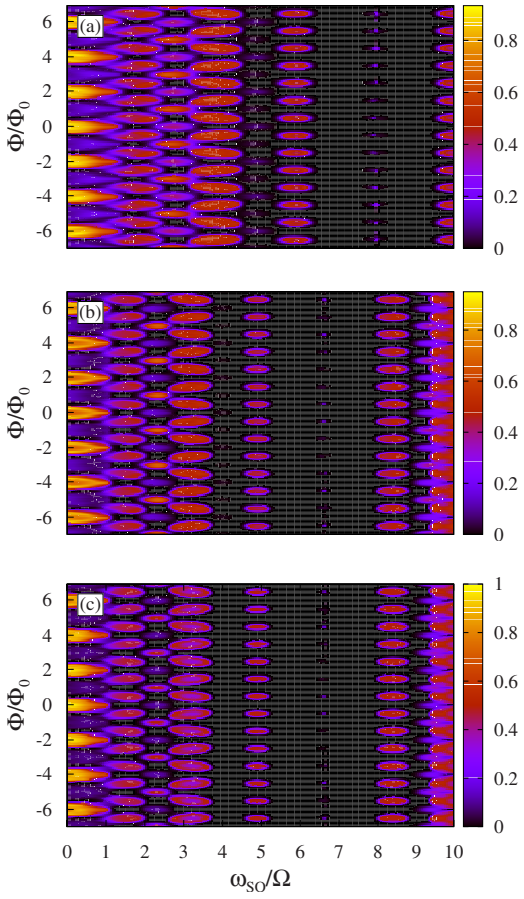

FIG. 4. (Color online) The conductance G/G_0 ($G_0=e^2/h$) of (a) 3×3, (b) 4×4, and (c) 5×5 rectangular arrays with 3, 4, and 5 input terminals, respectively, for $ka=19.6$ as a function of the SOI strength and the magnetic flux Φ (in units of $\Phi_0=h/e$).

strength ω_{SO}/Ω and ka. The values of ka are varied around $k_Fa=20.4$, corresponding to a Fermi energy of 11.13 meV in case of an effective mass $m^*=0.023m$ of InAs and rings of radius $a=0.25$ μm. In two-dimensional electron systems within an InAs quantum well, the value of α can be varied[2,3] up to 40 peV m. The different arrays show similar behavior for larger values of the SOI strength; there are slightly downward bending stripes (initially around even values of ka) where the devices are completely opaque for the electrons and also conducting regions which are initially around odd values of ka and have complex internal structure. Comparing our results to the case of a single ring with diametrically coupled leads,[11] it can be seen that the overall periodicity as a function of ka is determined by single-ring interferences. The increasing number of the rings causes modulations superimposing on the single-ring behavior. This point is probably the most apparent if we recall[11] that zero conductance areas are simply lines on the $ka-\omega_{SO}/\Omega$ plane for a single two-terminal ring, while in our case there are stripes, the width of which is slightly increasing with the size of the array. This effect is related to the increasing number of consecutive partially destructive interferences that finally lead to essentially zero currents at the outputs. Additionally, if we considered an infinite network, the periodic boundary conditions would allow only discrete values of ka for a given SOI strength with nonzero conductance. These conducting lines in the infinite case are situated on the $ka-\omega_{SO}\Omega$ plane around the middle of the conducting stripes shown in Fig. 3. Thus the results presented in this figure demonstrate a transition between the conductance properties of a single ring and that of an infinite network. In Sec. III B we will analyze the effect of pointlike scatterers on the nonconducting stripes shown in Fig. 3.

Focusing on small values of ω_{SO}/Ω, Fig. 3 shows a narrowing of the nonconducting regions until they eventually disappear when no SOI is present. Here the conductance still depends on ka, but its minimal values are not zeros and a periodic behavior can be seen; for a network of $N\times N$ rings, there are N minima as the value of ka is increased by 1. This size-dependent modulation is related to the horizontal extent of the device; if we compare the conductance of the networks to that of rings of the same size and number without vertical connections, the same periodic behavior can be seen around zero SOI.

Figure 4 shows the normalized magnetoconductance of networks of 3×3, 4×4, and 5×5 quantum rings for $ka=19.6$ as a function of the SOI strength and the magnetic flux Φ (measured in units of Φ_0). When ω_{SO}/Ω is zero, Aharonov-Bohm (AB) oscillations appear. For larger values

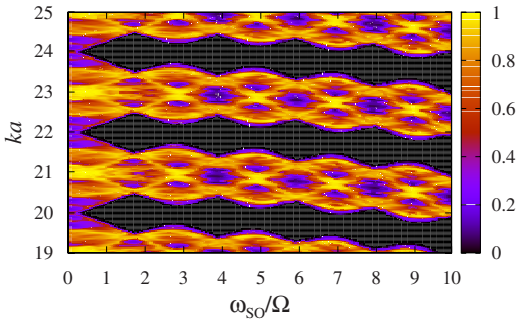

FIG. 5. (Color online) The conductance G/G_0 ($G_0=e^2/h$) of a 5×5 rectangular array with a single input lead attached to ring {31} for zero magnetic flux as a function of the SOI strength and ka.

of ω_{SO}/Ω both AB and Aharonov-Casher[28] oscillations can be seen in the magnetoconductance. As Fig. 4 was plotted for a certain value of ka, the effect of the bending nonconducting stripes seen in Fig. 3 can also be seen as the suppression of the conductance oscillations when such a stripe is reached due to the change in the SOI strength and their appearance again when the stripe is left. We note that for larger values of ka this bending effect is less pronounced.

Figures 5 and 6 show the conductance of a 5×5 network with a single input lead in the middle (i.e., attached to ring {31} using the notations of Fig. 2) as a function of ka and ω_{SO}/Ω (Fig. 5) and the magnetic field and ω_{SO}/Ω (Fig. 6). The overall structure of these plots remains the same as in the case when the current can enter through all the rings on the left-hand side, but the different boundary conditions modify the fine structure of the plots.

Our method allows the calculation of the spin directions for the different output terminals, and we found that spin-dependent interference in the array results in nontrivial spin transformations. Figure 7 shows the spin-resolved transmission probabilities for a 5×5 ring array with a single input lead. The incoming spin state is chosen to be $|\uparrow_z\rangle$, i.e., the spin-up eigenstate of σ_z, and the contour plots show the probabilities of the $|\uparrow_x\rangle$, $|\uparrow_y\rangle$, and $|\uparrow_z\rangle$ outputs at ring {55} on the right-hand side. The fact that the $|\uparrow_z\rangle$ input spinor changes its direction (as it is seen in Fig. 7, it can be transformed into $|\uparrow_x\rangle$ or $|\uparrow_y\rangle$) is due to the SOI induced spin rotations. The actual values of the spin-resolved transmission

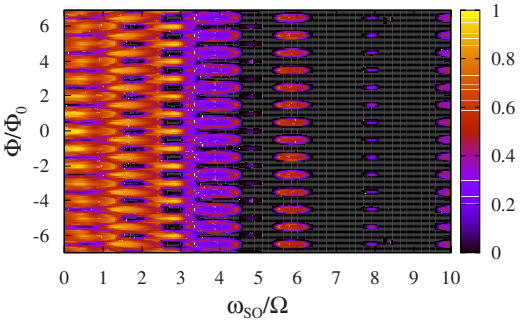

FIG. 6. (Color online) The conductance G/G_0 ($G_0=e^2/h$) of a 5×5 rectangular array with a single input lead attached to ring {31} for $ka=19.57$ as a function of the SOI strength and the magnetic flux Φ (in units of $\Phi_0=h/e$).

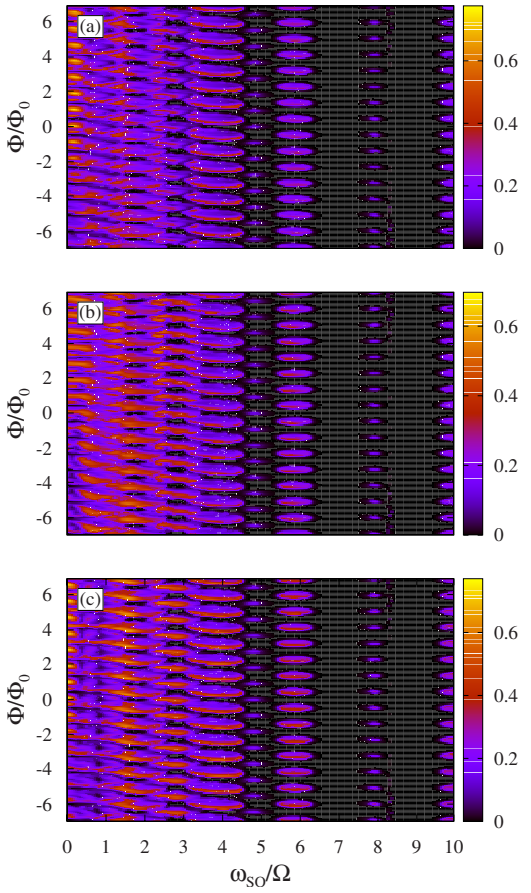

FIG. 7. (Color online) The probabilities of the (a) $|\uparrow_x\rangle$, (b) $|\uparrow_y\rangle$, and (c) $|\uparrow_z\rangle$ outputs at ring {55} of a 5×5 rectangular array with one input lead (attached to ring {31}) for $ka=19.6$ as a function of the SOI strength and the magnetic flux Φ (in units of $\Phi_0=h/e$). The incoming spin state is chosen to be $|\uparrow_z\rangle$.

probabilities are determined by the spin-dependent interference phenomena. Figure 8 shows the z component of the normalized output spinors and visualizes that spin-resolved results depend on the input side geometry as well. As we can see, the spin components change in the whole available range between -1 and 1, and their behavior is rather different for the cases when the electron can enter the array through any of the five terminals or only through the one attached to ring {31}. This phenomenon together with other spin-dependent interference effects[38–44] can lead to spin sensitive quantum networks.

B. Effect of pointlike scatterers

Now we will investigate to what extent the conductance properties are modified by the presence of random scatterers. Although high mobility samples have already become available (such that at cryogenic temperatures transport is found to be ballistic over tens of microns), considering also the effects caused by scattering events provides a more realistic description for most cases. To this end we introduce pointlike scattering centers between the rings. Note that attaching leads to rings and different rings to each other may lead to scattering, which is why the scattering centers are chosen to

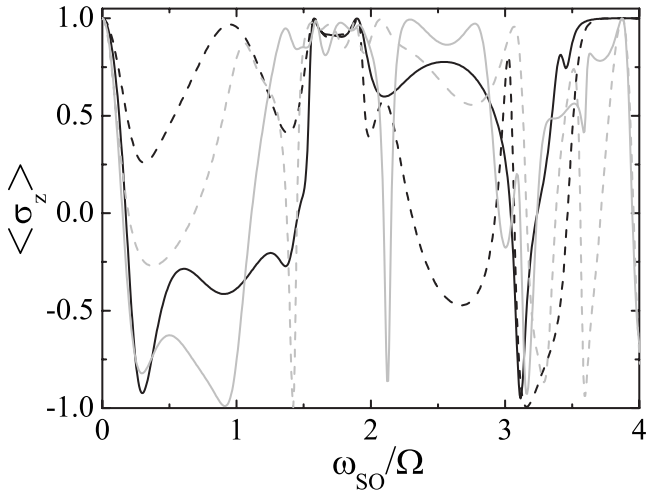

FIG. 8. The spin transformation properties of a 5×5 array with input leads attached to all rings and only to ring {31} (black and gray curves, respectively). The z component of the normalized spin states transmitted via the output terminals attached to ring {25} (solid line) and ring {45} (dashed line). The incoming spin state is chosen to be $|\uparrow_z\rangle$.

be placed in the junctions. At the end of this section we shall return to the question to what extent the transmission properties depend on the positions of the scattering centers.

At each point j where two rings touch each other, we consider an additional Dirac-delta potential of the form $\eta_j\delta(j)$. Here η_j represent independent normally distributed random variables with zero mean and root-mean-square deviation D. By tuning D we can model weak disturbances (small D) as well as the case when frequent scattering events completely change the character of the transport process (corresponding to large values of D).

As shown in Fig. 9, the most general consequence of these random scattering events is the overall decrease in the conductance. However, for strong enough disturbance, more interesting effects can be seen, namely, the splitting of the AB peaks. Note that the scattering has the most dramatic

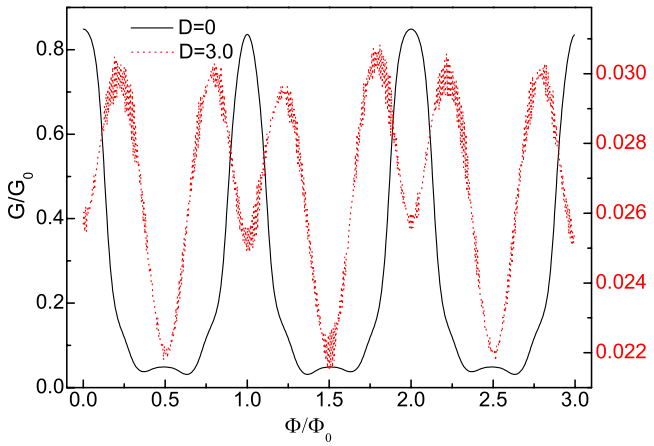

FIG. 9. (Color online) The conductance G (in units of $G_0=e^2/h$) of a 5×5 rectangular array with and without pointlike random scatterers between the rings as a function of the magnetic flux Φ (in units of $\Phi_0=h/e$) for $ka=20.2$ and $\omega_{SO}/\Omega=13.0$.

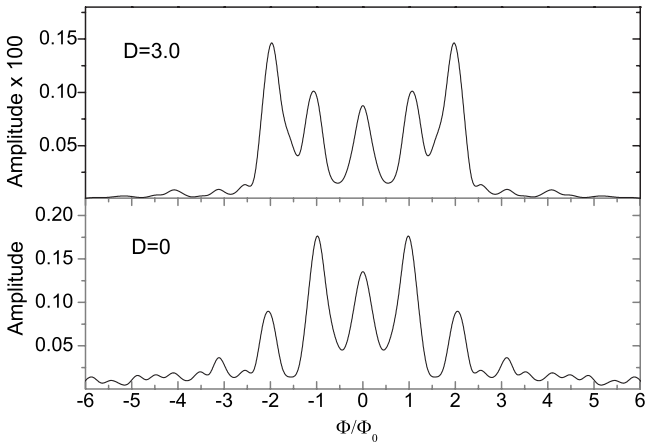

FIG. 10. Fourier spectra of the data shown in Fig. 9. Notice that the relative weight of peaks corresponding to $2\Phi/\Phi_0$ oscillations increases when scattering effects are introduced.

effect for the AB resonances, i.e., $\Phi=n\Phi_0$, and the least for the antiresonance condition, i.e., $\Phi=(n+1/2)\Phi_0$. We want to stress that the model we considered (random elastic-scattering processes in single-electron approximation) is similar to the case when the Al'tshuler-Aronov-Spivak (AAS) effect[45] is expected to survive in a single ring. Our results for a more complex geometry indicate similar physical consequences of the scattering events: introduction of new peaks in the AB oscillations. In fact, the Fourier spectrum of the conductance shown in Fig. 10 clearly indicates that for strong enough disturbance, the peaks corresponding to oscillations with a period of $2\Phi/\Phi_0$ are stronger than the AB peaks. Let us note that phenomena related to the AAS effect have recently been predicted for a single ring[46] and were detected in the case of ring arrays.[26]

Finally we return to the stripes shown in Fig. 3, where the conductance is negligible. According to Sec. III A, destructive interference is responsible for the appearance of these stripes. Therefore we expect that when scattering events destroy phase coherence, conductance should increase. This effect can be seen in Fig. 11, where the conductance is plotted as a function of the SOI strength for different root-mean-square deviations D of the random variables. As it is shown by this figure, for most values of ω_{SO}/Ω, the conductance is significantly increased in this region, although it is negligible in the exact ballistic case ($D=0$). On the other hand, however, G is practically zero around $\omega_{SO}/\Omega=7.9$, independently from the strength of the disturbance. This effect is related to single-ring interferences: having investigated the currents and spinor valued wave functions in the network, we found that for this parameter set (ka, ω_{SO}, and Φ), the input rings ({11}–{51}) are essentially totally opaque for the electrons, i.e., they basically do not enter the second column of the network. Clearly, in this case scattering centers in the junctions cannot modify the transmission properties. However, this kind of effects appears only for certain special parameter sets. We found that the positions of the scattering centers for a single ring are important, but in a system of two rings this effect is already remarkably weaker. The transmission properties of larger arrays are usually determined by global (i.e.,

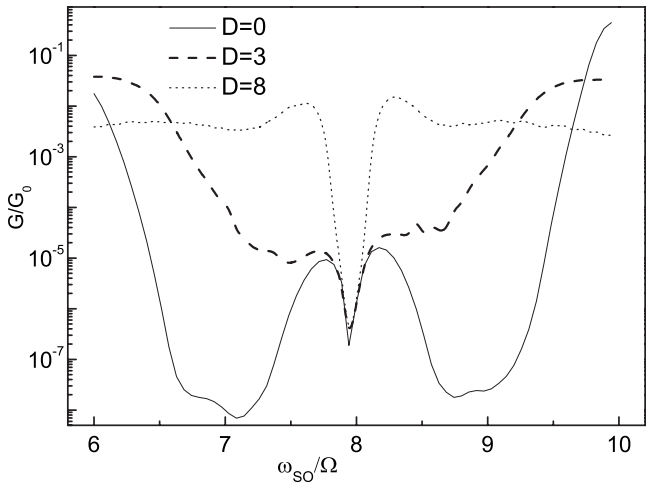

FIG. 11. The conductance G (in units of $G_0=e^2/h$) of a 5×5 rectangular array with pointlike random scatterers between the rings for different root-mean-square deviations D as a function of the SOI strength for $ka=19.6$ and $\Phi=0.3\Phi_0$.

involving all the rings) interferences when for strong enough disturbance the positions of the scattering centers play usually no significant role.

IV. SUMMARY

In this paper we calculated the spin-dependent transport properties of two-dimensional ring arrays. We applied general boundary conditions for the case of single-quantum rings, which allowed the construction of arrays of such rings as building blocks. The magnetoconductance of two-dimensional arrays of 3×3, 4×4, and 5×5 quantum rings exhibited Aharonov-Bohm and Aharonov-Casher oscillations.[28] We also determined the spin-resolved transmission probabilities of the arrays and found significant spin rotations depending on the SOI strength. We introduced pointlike random scattering centers between the rings, which, for strong enough disturbance, resulted in the splitting of the AB peaks. We note that an array of quantum rings with local (ring by ring) modulation of the SOI can lead to novel effects in spin state transformation of electrons.[47]

ACKNOWLEDGMENTS

This work was supported by the Flemish-Hungarian Bilateral Programme, the Flemish Science Foundation (FWO-Vl), the Belgian Science Policy, and the Hungarian Scientific Research Fund (OTKA) under Contracts No. T48888, No. M36803, and No. M045596. P.F. was supported by a J. Bolyai grant of the Hungarian Academy of Sciences. We thank J. Sólyom for enlightening discussions.

APPENDIX

Here we present the detailed analytic expressions of the scattering problem for general two- and four-terminal rings, in which SOI and a perpendicular magnetic field are present, the latter of which is considered as a perturbation. As we have shown in Sec. II, it is sufficient to consider only one input terminal and determine the connection between the input and output states, i.e., the reflection and transmission matrices, since the more general boundary condition of having inputs on all terminals is just a superposition of such cases with an appropriate rotation of the matrices [see Eqs. (10) and (11)]. Considering f_1 as the only input [i.e., $f_{i\neq1}=0$, in Figs. 1(a) and 1(c)], requiring the continuity of the wave functions, and applying Griffith boundary conditions[32,37] at the junctions in both cases, we can obtain the reflection matrices $\hat{R}^{f_1}$ and $\tilde{R}^{f_1}$ of the two-terminal ring and of the four-terminal ring, respectively. Both can be written in a form analogous to that of R^{f_1} of the three-terminal case given by Eq. (7) with

$$\hat{\varrho}^{(\mu)}=\frac{4k^2a^2}{\hat{y}^{(\mu)}}\{\sin(q^{(\mu)}\gamma_1)\sin(q^{(\mu)}(2\pi-\gamma_1))+iq^{(\mu)}\sin(2q^{(\mu)}\pi)\}$$

and

$$\begin{aligned}\tilde{\varrho}^{(\mu)}=&\frac{2ka}{\tilde{y}^{(\mu)}}\{k^3a^3[\cos(2q^{(\mu)}\pi)+\cos(2q^{(\mu)}(\pi-\gamma_3+\gamma_2-\gamma_1))-\cos(2q^{(\mu)}(\pi-\gamma_3+\gamma_2))+\cos(2q^{(\mu)}(\pi-\gamma_3+\gamma_1))\\&-\cos(2q^{(\mu)}(\pi-\gamma_2+\gamma_1))-\cos(2q^{(\mu)}(\pi-\gamma_3))+\cos(2q^{(\mu)}(\pi-\gamma_2))-\cos(2q^{(\mu)}(\pi-\gamma_1))]\\&+2ik^2a^2q^{(\mu)}[\sin(2q^{(\mu)}(\pi-\gamma_3+\gamma_2))-3\sin(2q^{(\mu)}\pi)+\sin(2q^{(\mu)}(\pi-\gamma_3+\gamma_1))+\sin(2q^{(\mu)}(\pi-\gamma_2+\gamma_1))]\\&+4ik^2a^2q^{(\mu)}[\sin(2q^{(\mu)}(\pi-\gamma_1))-\sin(2q^{(\mu)}(\pi-\gamma_3))]-4ka(q^{(\mu)})^2[\cos(2q^{(\mu)}(\pi-\gamma_3))+\cos(2q^{(\mu)}(\pi-\gamma_2))\\&+\cos(2q^{(\mu)}(\pi-\gamma_1))-3\cos(2q^{(\mu)}\pi)]-8i(q^{(\mu)})^3\sin(2q^{(\mu)}\pi)\},\end{aligned}$$

respectively. Here

$$\hat{y}^{(\mu)}=k^2a^2\{\cos[2q^{(\mu)}(\pi-\gamma_1)]-\cos[2q^{(\mu)}\pi]\}+4ikaq^{(\mu)}\sin[2q^{(\mu)}\pi]-4[q^{(\mu)}]^2\{\cos[[(-1)^{\mu+1}w+2\phi]\pi]+\cos[2q^{(\mu)}\pi]\},$$

$$\begin{aligned}\tilde{y}^{(\mu)}=&16(q^{(\mu)})^4\{\cos[[(-1)^{\mu+1}w+2\phi]\pi]+\cos[2q^{(\mu)}\pi]\}-32ika[q^{(\mu)}]^3\sin[2q^{(\mu)}\pi]+24k^2a^2[q^{(\mu)}]^2\cos[2q^{(\mu)}\pi]\\&-4k^2a^2[q^{(\mu)}]^2\{\cos[2q^{(\mu)}(\pi-\gamma_3)]+\cos[2q^{(\mu)}(\pi-\gamma_2)]+\cos[2q^{(\mu)}(\pi-\gamma_1)]+\cos[2q^{(\mu)}(\pi-\gamma_3+\gamma_1)]\\&+\cos[2q^{(\mu)}(\pi-\gamma_3+\gamma_2)]+\cos[2q^{(\mu)}(\pi-\gamma_2+\gamma_1)]\}-8ik^3a^3q^{(\mu)}\sin[2q^{(\mu)}\pi]+4ik^3a^3q^{(\mu)}[\sin[2q^{(\mu)}(\pi-\gamma_3+\gamma_2)]\end{aligned}$$

$$- \sin[2q^{(\mu)}(\pi - \gamma_3)] + \sin[2q^{(\mu)}(\pi - \gamma_2 + \gamma_1)] + \sin[2q^{(\mu)}(\pi - \gamma_1)]] + k^4a^4\{\cos[2q^{(\mu)}(\pi - \gamma_3 + \gamma_2 - \gamma_1)] + \cos[2q^{(\mu)}\pi]$$
$$+ \cos[2q^{(\mu)}(\pi - \gamma_3 + \gamma_1)] - \cos[2q^{(\mu)}(\pi - \gamma_3 + \gamma_2)] - \cos[2q^{(\mu)}(\pi - \gamma_2 + \gamma_1)] - \cos[2q^{(\mu)}(\pi - \gamma_3)]$$
$$+ \cos[2q^{(\mu)}(\pi - \gamma_2)] - \cos[2q^{(\mu)}(\pi - \gamma_1)]\},$$

where the angles γ_i are defined in Figs. 1(a) and 1(c). The transmission matrices $\hat{T}^{f_1}$ of the two-terminal ring and $\tilde{T}_n^{f_1}$ ($n=1,2,3$) of the four-terminal ring can be given in an analogous form to that of the transmission matrices $T_n^{f_1}$ of the three-terminal one given by Eq. (8) with

$$\hat{\tau}^{(\mu)} = \frac{4ikaq^{(\mu)}}{\hat{y}^{(\mu)}} e^{i\gamma_1((-1)^{\mu+1}w/2+\phi)}[\sin(q^{(\mu)}(2\pi - \gamma_1)) - e^{-i\pi((-1)^{\mu+1}w+2\phi)} \sin(q^{(\mu)}\gamma_1)],$$

and

$$\tilde{\tau}_1^{(\mu)} = \frac{4kaq^{(\mu)}}{\tilde{y}^{(\mu)}} e^{i\gamma_1/2((-1)^{\mu+1}w+2\phi)} \times \{ik^2a^2[\sin(q^{(\mu)}(2\pi - 2\gamma_3 + 2\gamma_2 - \gamma_1)) - \sin(q^{(\mu)}(2\pi - \gamma_1)) + \sin(q^{(\mu)}(2\pi - 2\gamma_2 + \gamma_1))$$
$$- \sin(q^{(\mu)}(2\pi - 2\gamma_3 + \gamma_1))] - 2kaq^{(\mu)}[\cos(q^{(\mu)}(2\pi - 2\gamma_2 + \gamma_1)) - 2\cos(q^{(\mu)}(2\pi - \gamma_1)) + \cos(q^{(\mu)}(2\pi - 2\gamma_3 + \gamma_1))]$$
$$+ 4i(q^{(\mu)})^2[e^{-i\pi((-1)^{\mu+1}w+2\phi)} \sin(q^{(\mu)}\gamma_1) - \sin(q^{(\mu)}(2\pi - \gamma_1))]\},$$

$$\tilde{\tau}_2^{(\mu)} = \frac{4kaq^{(\mu)}}{\tilde{y}^{(\mu)}} e^{i\gamma_2/2((-1)^{\mu+1}w+2\phi)}\{-2kaq^{(\mu)}[e^{-i\pi((-1)^{\mu+1}w+2\phi)} \cos(q^{(\mu)}\gamma_2) - e^{-i\pi((-1)^{\mu+1}w+2\phi)} \cos(q^{(\mu)}(2\gamma_1 - \gamma_2))$$
$$+ \cos(q^{(\mu)}(2\pi - 2\gamma_3 + \gamma_2)) - \cos(q^{(\mu)}(2\pi - \gamma_2))] + 4i(q^{(\mu)})^2[e^{-i\pi((-1)^{\mu+1}w+2\phi)} \sin(q^{(\mu)}\gamma_2) - \sin(q^{(\mu)}(2\pi - \gamma_2))]\},$$

$$\tilde{\tau}_3^{(\mu)} = \frac{4kaq^{(\mu)}}{\tilde{y}^{(\mu)}} e^{i\gamma_3/2((-1)^{\mu+1}w+2\phi)}\{ik^2a^2e^{-i\pi((-1)^{\mu+1}w+2\phi)}[\sin(q^{(\mu)}\gamma_3) + \sin(q^{(\mu)}(2\gamma_1 - \gamma_3)) - \sin(q^{(\mu)}(2\gamma_2 - \gamma_3))$$
$$+ \sin(q^{(\mu)}(2\gamma_2 - 2\gamma_1 - \gamma_3))] - 2kaq^{(\mu)}e^{-i\pi((-1)^{\mu+1}w+2\phi)}[2\cos(q^{(\mu)}\gamma_3) - \cos(q^{(\mu)}(2\gamma_1 - \gamma_3)) - \cos(q^{(\mu)}(2\gamma_2 - \gamma_3))]$$
$$+ 4i(q^{(\mu)})^2[e^{-i\pi((-1)^{\mu+1}w+2\phi)} \sin(q^{(\mu)}\gamma_3) - \sin(q^{(\mu)}(2\pi - \gamma_3))]\},$$

respectively.

*benedict@physx.u-szeged.hu

[1] M. König, A. Tschetschetkin, E. M. Hankiewicz, J. Sinova, V. Hock, V. Daumer, M. Schäfer, C. R. Becker, H. Buhmann, and L. W. Molenkamp, Phys. Rev. Lett. **96**, 076804 (2006).
[2] D. Grundler, Phys. Rev. Lett. **84**, 6074 (2000).
[3] J. Nitta, T. Akazaki, H. Takayanagi, and T. Enoki, Phys. Rev. Lett. **78**, 1335 (1997).
[4] Y. Sato, S. G. T. Kita, and S. Yamada, J. Appl. Phys. **89**, 8017 (2001).
[5] J. Splettstoesser, M. Governale, and U. Zülicke, Phys. Rev. B **68**, 165341 (2003).
[6] J. S. Sheng and K. Chang, Phys. Rev. B **74**, 235315 (2006).
[7] S. R. Eric Yang, Phys. Rev. B **74**, 075315 (2006).
[8] L. W. Yu, K. J. Chen, J. Song, J. Xu, W. Li, X. F. Li, J. M. Wang, and X. F. Huang, Phys. Rev. Lett. **98**, 166102 (2007).
[9] M. Büttiker, Y. Imry, and M. Y. Azbel, Phys. Rev. A **30**, 1982 (1984).
[10] J. Nitta, F. E. Meijer, and H. Takayanagi, Appl. Phys. Lett. **75**, 695 (1999).
[11] B. Molnár, F. M. Peeters, and P. Vasilopoulos, Phys. Rev. B **69**, 155335 (2004).
[12] D. Frustaglia and K. Richter, Phys. Rev. B **69**, 235310 (2004).
[13] P. Földi, B. Molnár, M. G. Benedict, and F. M. Peeters, Phys. Rev. B **71**, 033309 (2005).
[14] X. F. Wang and P. Vasilopoulos, Phys. Rev. B **72**, 165336 (2005).
[15] S. Souma and B. K. Nikolić, Phys. Rev. Lett. **94**, 106602 (2005).
[16] Y. K. Kato, R. C. Myers, A. C. Gossard, and D. D. Awschalom, Appl. Phys. Lett. **86**, 162107 (2005).
[17] S. Bellucci and P. Onorato, J. Phys.: Condens. Matter **19**, 395020 (2007).
[18] B. Szafran and F. M. Peeters, Phys. Rev. B **72**, 165301 (2005).
[19] P. Vasilopoulos, O. Kálmán, F. M. Peeters, and M. G. Benedict, Phys. Rev. B **75**, 035304 (2007).
[20] J. B. Yau, E. P. DePoortere, and M. Shayegan, Phys. Rev. Lett. **88**, 146801 (2002).
[21] D. Frustaglia, M. Hentschel, and K. Richter, Phys. Rev. Lett. **87**, 256602 (2001).
[22] G. Cohen, O. Hod, and E. Rabani, Phys. Rev. B **76**, 235120 (2007).
[23] B. Molnár, P. Vasilopoulos, and F. M. Peeters, Phys. Rev. B **72**, 075330 (2005).
[24] E. I. Rashba, Sov. Phys. Solid State **2**, 1109 (1960).
[25] T. Koga, J. Nitta, T. Akazaki, and H. Takayanagi, Phys. Rev.

Lett. **89**, 046801 (2002).
[26] T. Bergsten, T. Kobayashi, Y. Sekine, and J. Nitta, Phys. Rev. Lett. **97**, 196803 (2006).
[27] Z. Zhu, Y. Wang, K. Xia, X. C. Xie, and Z. Ma, Phys. Rev. B **76**, 125311 (2007).
[28] Y. Aharonov and A. Casher, Phys. Rev. Lett. **53**, 319 (1984).
[29] S. Datta, *Electronic Transport in Mesoscopic Systems* (Cambridge University Press, Cambridge, England, 1995).
[30] P. Földi, B. Molnár, M. G. Benedict, and F. M. Peeters, Phys. Rev. B **71**, 033309 (2005).
[31] A. G. Aronov and Y. B. Lyanda-Geller, Phys. Rev. Lett. **70**, 343 (1993).
[32] J. B. Xia, Phys. Rev. B **45**, 3593 (1992).
[33] P. Földi, O. Kálmán, M. G. Benedict, and F. M. Peeters, Phys. Rev. B **73**, 155325 (2006).
[34] O. Kálmán, P. Földi, and M. G. Benedict, Open Syst. Inf. Dyn. **13**, 455 (2006).
[35] O. Kálmán, P. Földi, M. G. Benedict, and F. M. Peeters, Physica E (Amsterdam) **40**, 567 (2008).
[36] F. E. Meijer, A. F. Morpurgo, and T. M. Klapwijk, Phys. Rev. B **66**, 033107 (2002).
[37] S. Griffith, Trans. Faraday Soc. **49**, 345 (1953).
[38] A. Pályi and J. Cserti, Phys. Rev. B **76**, 035331 (2007).
[39] J. Cserti, A. Csordás, and U. Zülicke, Phys. Rev. B **70**, 233307 (2004).
[40] T. Koga, J. Nitta, and M. van Veenhuizen, Phys. Rev. B **70**, 161302(R) (2004).
[41] R. Ionicioiu and I. D'Amico, Phys. Rev. B **67**, 041307(R) (2003).
[42] U. Zülicke and A. I. Signal, Solid State Commun. **144**, 529 (2007).
[43] A. W. Cummings, R. Akis, and D. K. Ferry, Appl. Phys. Lett. **89**, 172115 (2006).
[44] S. Bellucci and P. Onorato, Phys. Rev. B **77**, 165305 (2008).
[45] B. L. Al'tshuler, A. G. Aronov, and B. F. Spivak, JETP Lett. **33**, 94 (1981).
[46] M. J. van Veenhuizen, T. Koga, and J. Nitta, Phys. Rev. B **73**, 235315 (2006).
[47] P. Földi, O. Kálmán, M. G. Benedict, and F. M. Peeters, Nano Lett. **8**, 2556 (2008).